Available online at www.sciencedirect.com

jmr&t Journal of Materials Research and Technology

https://www.journals.elsevier.com/journal-of-materials-research-and-technology

Original Article

Microstructural characterisation and mechanical properties of dissimilar AA5083-copper joints produced by friction stir welding

Gihad Karrar[a,*], *Alexander Galloway*[a], *Athanasios Toumpis*[a], *Hongjun Li*[b], *Fadi Al-Badour*[c]

[a] *Department of Mechanical & Aerospace Engineering, University of Strathclyde, Glasgow G1 1XJ, UK*

[b] *Faculty of Mechanical Engineering and Automation, Zhejiang Sci-Tech University, Xiasha Higher Education Zone, Hangzhou 310018, PR China*

[c] *Mechanical Engineering Department, King Fahd University of Petroleum and Minerals, Dhahran, 31261, Saudi Arabia*

ARTICLE INFO

Article history:
Received 10 May 2020
Accepted 16 August 2020

Keywords:
Intermetallic compounds
Friction stir welding
Mechanical properties
Dissimilar joining
AA5083
Commercially pure copper.

ABSTRACT

This work aims to study the influence of the tool rotational speed and tool traverse speed on dissimilar friction stir butt welds on 3 mm thick AA5083 to commercially pure copper plates. Complex microstructures were formed in the thermo-mechanically affected zone, in which a vortex-like pattern and lamellar structures were found. Several intermetallic compounds were identified in this region, such as Al2Cu, Al4Cu9 and these developed an inhomogeneous hardness distribution. The highest ultimate tensile strength of 203 MPa and joint efficiency of 94.8% were achieved at 1400 rpm tool rotational speed and 120 mm/min traverse speed. Placing the softer material (aluminium) on the advancing side produced an excellent metallurgical bond with no requirement for tool offsetting.

1. Introduction

Dissimilar aluminium/copper joints are commonly used where there are advantages in partially replacing the copper with aluminium for certain engineering applications such as electrical connectors, tubes of heat exchangers, transformer's foil conductors and capacitor foil windings [1–4]. This is largely driven by the similarities in the electrical properties of each metal. Beyond this, the reduced cost and the lower mass of aluminium renders it an attractive partial substitute for copper [5–7]. In circumstances where there is a need to weld the substitute aluminium part to pure copper, significant challenges emerge as a result of the differences in chemical compositions and the mismatch in the physical and mechanical properties of each metal [8–10]. Based on the relative advantages against conventional fusion welding processes, i.e. absence of porosity, solidification cracking, oxidation and lower distortion [11–14], the friction stir welding (FSW) technique can replace the conventional joining methods due to its capability to produce defect-free weld on dissimilar metals and alloys [15–17].

* *Corresponding author.*
E-mail: gihad-mohamed-karrar-babekr@strath.ac.uk (G. Karrar).

https://doi.org/10.1016/j.jmrt.2020.08.073

Ouyang et al. [18] studied the microstructural evolution during friction stir butt welding of AA6061-T6 to copper, in which the latter was placed on the advancing side (AS). As a general note, they claimed that FSW of aluminium to copper was difficult due to the formation of brittle intermetallic compounds (IMCs) which led to poor mechanical properties. In their studies [18], the dissimilar mechanically mixed zone i.e. stir zone and thermo-mechanically affected zone (TMAZ) exhibited a complex microstructure with several IMCs such as Al2Cu, CuAl and Al4Cu9. However distinctive microhardness levels were observed at the stir zone, and there was a lack of further investigation on the joint mechanical properties. Abdollah-Zadeh et al. [19] studied the effect of tool rotational speed and tool traverse speed on the microstructure and mechanical properties of the joint by only considering the lap configuration. The existence of Al2Cu, CuAl and Al4Cu9 IMCs was also confirmed as in the aforementioned study [18]. The study [19] concluded that a suitable rotational to traverse speed ratio resulted in maximising the joint mechanical properties. Furthermore, the relationship between IMC formation and joint mechanical strength has been investigated by Xue et al. [20] at different tool offsets, tool rotational and traverse speeds of dissimilar AA1060 aluminium to pure copper joints. Noticeable improvements in the ultimate tensile strength (UTS) were observed when the IMC thickness increased, especially at the interface between the aluminium base metal and the stir zone. Their findings [20] were in agreement with other studies [21–24], whereas other published work [25,26] proposed that the joint mechanical strength depended on the volume fraction, geometry and distribution of the IMCs.

An additional key factor that affects the joint mechanical properties in FSW of aluminium to copper is the placement of each workpiece [27]. Numerous studies noted that defect-free butt joints between aluminium to copper could be produced by placing the harder material (copper) on the AS [28–30]. According to these studies [28–30], placing the copper on the AS leads to suitable mixing between the aluminium and copper since it is easier for the softer material (aluminium) to flow. However, tool offsetting towards either retreating or advancing side was usually required to achieve defect-free joints [31]. The various ranges reported for the tool offsets resulted in this method being impractical for industrial use.

In contrast, other researchers reported that sound joints may be obtained by placing the softer material (aluminium) on the advancing side [32–35]. For example, Tan et al. [32] successfully joined 3 mm thick 5A02 aluminium to copper by placing the aluminium on the advancing side and negligible tool offset towards the advancing side. Tool rotational speed of 1100 rpm and 20 mm/min tool traverse speed were the welding parameters that resulted in a high UTS of 130 MPa (75.6% joint efficiency relative to the aluminium base metal). According to their findings [32], the presence of a thin and continuous layer of IMCs was observed at the aluminium/copper interface. The formation of these IMCs was also detected inside the stir zone and resulted in an inhomogeneous hardness distribution across the weld. Further, they noted that a channel defect developed at a higher tool traverse speed of 40 mm/min.

Despite the advantages on the joint mechanical properties when placing the softer material (aluminium) on the advancing side, limited research has focused on this configuration. Additionally, the relationship between the IMCs microstructure and the mechanical properties requires further investigations. In this paper, the influence of tool rotational and traverse speed on the joint quality has been evaluated when placing the aluminium on the advancing side and without introducing the complexities of tool offsetting. Using this configuration, three parameter sets of rotational and traverse speed were employed to investigate the relationship between microstructure and mechanical properties.

Table 1 – Chemical composition (in wt.%) of AA5083.

Si	Mg	Cu	Mn	Zn	Ti	Cr	Fe
0.98	4.0	0.10	0.70	0.25	0.15	0.10	0.40

Table 2 – Chemical composition (in wt.%) of commercially pure copper.

Cu	Ag	Fe	Bi	Sb	As	Pb	S
Bal	0.035	0.05	0.001	0.002	0.002	0.005	0.005

Table 3 – Mechanical properties of base metals.

Materials	Yield strength (MPa)	UTS (MPa)	EL (%)	Avg. HV
AA5083	163.97	225.66	67.57	70
Copper	257.26	273.66	114.14	90

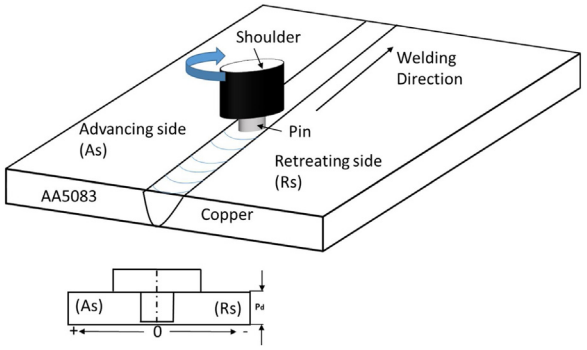

Fig. 1 – Experimental set-up.

2. Experimental programme

2.1. *Materials and FSW details*

A fully instrumented HT-JM16 × 8/2 static gantry FSW machine was used to butt weld 150 × 50 × 3 mm thick AA5083 to commercially pure copper plates along their lengths. A simple high strength steel tool design was used for welding. The tool pin diameter (Dp) and pin length (plunging depth, Pd) were 4.5 mm and 2.7 mm respectively, while the shoulder diameter (Ds) was 18 mm. The chemical compositions, as well as the mechanical properties of the two materials are presented in Tables 1, 2 and 3. A schematic illustration of the experimental set-up is shown in Fig. 1. After preliminary trials, defect-free joints were obtained when positioning the soft

Table 4 – Summary of the FSW process parameters.

Test No.	Rotational speed (rpm)	Traverse speed (mm/min)	ω/ν ratio (rev/mm)
1	1000	80	12.5
2	1000	100	10
3	1000	120	8.3
4	1200	80	15
5	1200	100	12
6	1200	120	10
7	1400	80	17.5
8	1400	100	14
9	1400	120	11.7

material (AA5083) at the advancing side with 0 mm tool offset, therefore, the main purpose of this work is to optimise the process parameters when different rotational and traverse speeds (ω/ν ratio) are used (Table 4). During FSW, the tool was tilted by an angle of 2.8°.

2.2. *Metallographic examination*

Following welding, samples were metallographically prepared using standard metallographic techniques. Etching was performed using a solution of 1 g of FeCl3, 10 mL HCl, and 100 mL distilled water to first reveal the copper side, following which the AA5083 side was etched for 60 s in a solution consisting of 1 g NaCl and 50 mL H3PO4 dissolved in 125 mL of ethanol, followed by a 12 s step using Wecks's tint (4 g of KMnO4 and 1 g of NaOH dissolved in 100 mL of distilled water). Thereafter, each etched sample was examined with the aid of high-resolution optical microscopy. In terms of compositional analysis and phase identification, energy dispersive spectroscopy (EDS) and X-ray diffraction (XRD) were performed at various locations of the weld joint. XRD was performed with a 40-mA operating current, 40-Kv voltage and 1.5406-Å Cu Kα radiation. A scanning rate of 0.02 deg./step within the range of $20^\circ < 2\theta < 100^\circ$ was used throughout.

2.3. *Mechanical testing*

The joint mechanical strength was investigated in accordance with ASTM-E8, details of which are shown in Fig. 2. The technique of hardness mapping was also employed to establish the relationship between IMCs formation and joint mechanical strength.

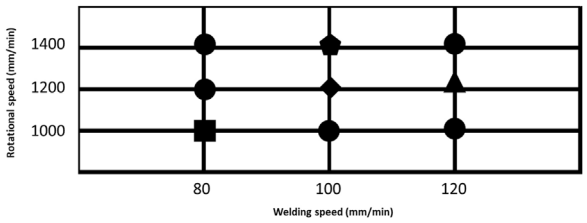

Fig. 3 – Effect of tool rotational and traverse speed on macrostructure.

3. Results and discussions

3.1. *Weld appearance and macrostructure*

Table 5 shows the typical top surface weld appearance and cross-sectional macrostructures of AA5083 to copper dissimilar metal FSW joints at different welding conditions. The symbols for each defect type relate to Fig. 3. As expected, the weld surface quality is indicative of the tendency for volumetric defects to develop [26]. For instance, excessive flash formation, as well as material discontinuity, will generally suggest volumetric defects [29]. Fig. 3 summarises the effect of tool rotational and traverse speed on the weld appearance and macrostructure, in which AA5083 was placed on the AS without tool offset. When the rotational speed varied from 1000 to 1400 rpm and the traverse speed was in the range of 80–120 mm/min, visually acceptable welds with no surface defects were obtained at the following specific parameter sets:

- Low rotational speed level of 1000 rpm at 100 mm/min and 120 mm/min welding speeds (10 and 8.3 ω/ν ratio) i.e. test no. 2 and 3 respectively.
- Intermediate rotation rate level of 1200 rpm and 80 mm/min (15 ω/ν ratio).
- High rotation rate level of 1400 rpm for the two ranges of the welding speed 80, and 120 mm/min (17.5, and 11.7 ω/ν ratio), respectively.

Parameter sets outside the above conditions led to an uneven surface and the formation of defects such as macrocracks towards the retreating side (copper, Fig. 4 (a)), cavities with a certain defect area on the cross-section less than 0.02 mm^2 (Fig. 4 (b)), voids (Fig. 4 (c)) and tunnel defects in which

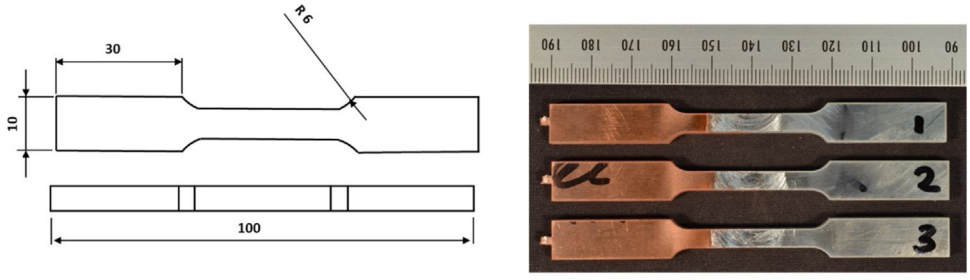

(a) (b)

Fig. 2 – (a) Dimensions of the tensile sample as per ASTM E8 standards. (b) Example of samples through the welding direction at 1000 rpm and 100 mm/min.

Table 5 – Weld appearance and macrostructure of dissimilar joints (marks as in Fig.3).

Symbol	Defect	Appearance and Macrostructure	Microstructure
●	None	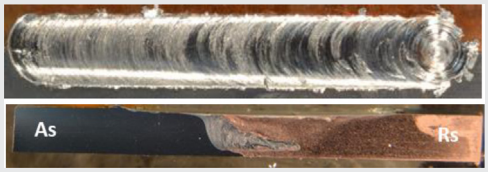	–
⬟	Crack	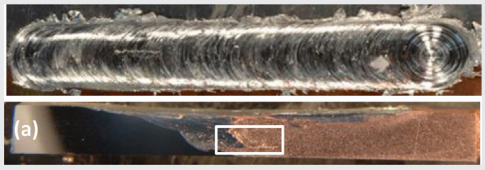	Fig. 4 (a)
◆	Cavity	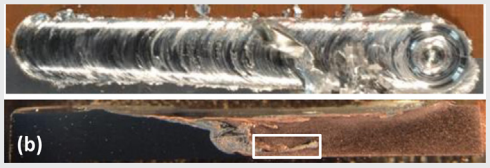	Fig. 4 (b)
■	Void	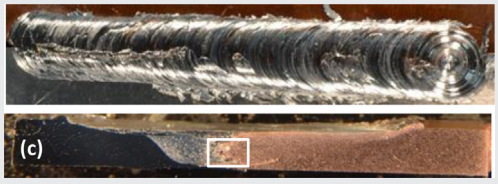	Fig. 4 (c)
▲	Tunnel	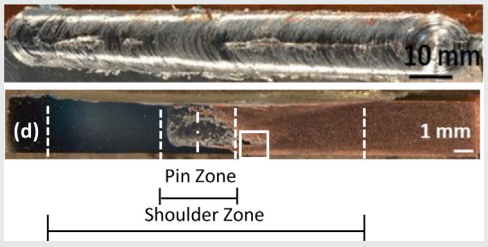	Fig. 4 (d)

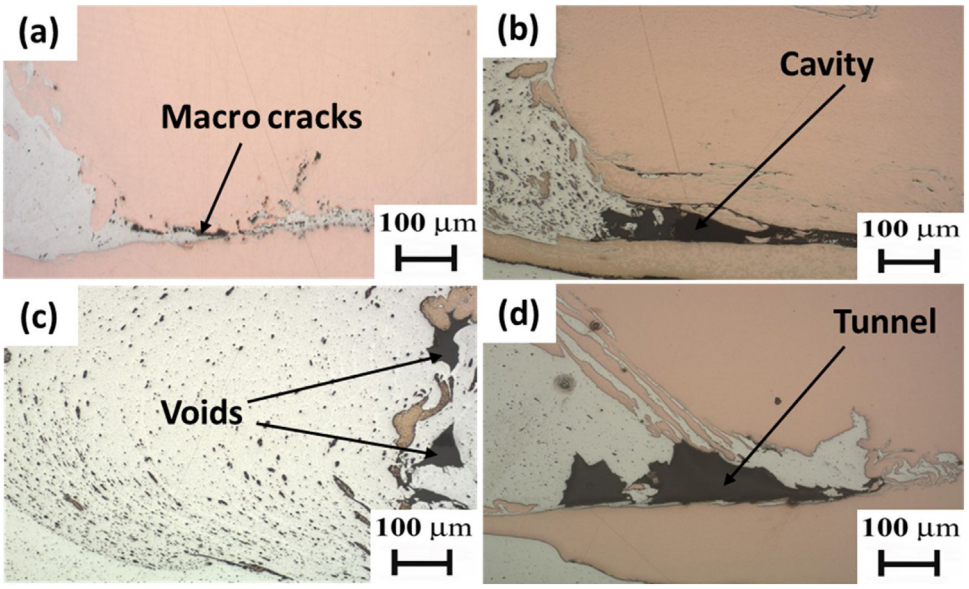

Fig. 4 – Magnified views for different defects on regions marked in Table 5.

Table 6 – EDS results at weld stir zone of Test no. 2.

Position	Al	Cu	Non equilibrium solid solution
1	75.14	24.86	–
2	62.76	37.24	–
3	90.35	9.65	Al (Cu)
4	85.84	14.16	Al (Cu)
5	61.98	38.02	–
6	68.08	31.92	–
7	67.18	32.82	–
8	79.26	20.74	–
9	37.72	62.28	–
10	35.22	64.78	–

the defect area was larger than 0.05 mm^2 (Fig. 4 (d)). Due to the inappropriate material flow, these types of defects have previously been reported [31], where the cracks are usually related to the formation of large IMC particles, cavities, voids and tunnel defects.

3.2. *Microstructural analysis*

The weld mechanical integrity is directly related to the stir zone microstructure. A classical "onion ring" structure is commonly found in the stir zone of similar material FSW joints [23]. In dissimilar material FSW however, a swirl-like pattern, banded or lamella structure, as well as vortex-type microstructures, are formed in the stir zone, TMAZ and also in the heat-affected zone (HAZ) [31]. Fig. 5 (a) represents an example of a typical cross-section of AA5083 (AS) to copper dissimilar metal FSW joint welded at 1000 rpm and 100 mm/min. Towards the aluminium side (Fig. 5 (b&e)), relatively small copper particles were observed as regularly distributed between the aluminium interface zone and the upper surface of the stir zone. Fig. 5 (c&f) illustrate that at the stir zone, larger copper particles (fragments) were stretched and irregularly distributed along the stir zone and towards the bottom of the interfacial region between the stir zone and the copper side. The irregular copper particles created a lamella structure of copper and aluminium at the bottom of the TMAZ towards the copper side (Fig. 5 (d&g)).

EDS analysis was performed to reveal the variation on the aluminium and copper content at 1000 rpm, 100 mm/min and 10 ω/v (see Test no. 2 of Table 4). It can be revealed from Fig. 6 (a) and Table 6 that good intermixing between aluminium and copper was achieved. Table 6 also shows the presence of different aluminium solid solutions at this low level of rotational speed. Fig. 6 (e) presents an example of how the EDS analysis was performed to capture the variation on the aluminium and copper content. Unetched microstructures for the distinctive regions from Fig. 6 (a): Al-stir zone (rectangular i), inside the stir zone (rectangular ii) as well as Cu-stir zone (rectangular iii), are presented in Fig. 6 (b), (c) and (d), respectively. The dark shaded layers surrounding the copper particles and fragments demonstrate the formation of the Al/Cu intermixed region as shown by the arrows. This embedded layer was previously reported to accompany the formation of Al/Cu IMCs [29]. Moderate stirring action was observed on the copper particles and fragments, which indicates the absence of the composite-like structure under this condition. Additionally, detached copper pieces failed to react with the aluminium matrix on the advancing side resulting in the absence of any lamella or banded structures at the interface zone.

Table 7 – EDS results at weld stir zone condition 7.

Position	Al	Cu
1	76.5	23.5
2	71.7	28.3
3	55.27	44.73
4	62.62	37.38
5	67.38	32.64
6	33.72	66.28

A cross-section of an AA5083 to copper defect-free joint at a higher level of rotational speed is shown in Fig. 7 (a), as-welded at 1400 rpm and 80 mm/min with AA5083 on AS and no tool offset. Although three distinctive regions can still be observed across the weld joint, these regions were completely different from the example of lower welding speed, i.e. 1000 rpm. The complex structure has formed in the aluminium side of the interface and towards the stir zone as shown in Fig. 7 (b&e). Copper fragments were detached from the retreating side and stirred with the aluminium matrix to create this complex structure. A higher heat input is the reason behind this complex structure, where the stirring action was insufficient to create this structure at a lower level of rotational speed. Evidence of the relationship between the heat input and the plastic stirring action was also observed inside the stir zone in Fig. 7 (c&f) and this resulted in the swirl and vortex-like structure. Unlike others [33–35], placing the copper on the retreating side without tool offset produced a wider TMAZ at the Al/Cu interface as illustrated in Fig. 7 (d&g).

Likewise, EDS was applied at different positions on the weld zone as illustrated in Fig. 8 (a), where Table 7 summarises the elemental compositions at these points, Fig. 8 (e) demonstrates an example of these EDS points. Table 7 shows the variation in Al/Cu contents as a result of good intermixing and the absence of non-equilibrium solid solutions. An enlarged view of rectangle (i) in Fig. 8 (a) is shown in Fig. 8 (b). A complex structure can be detected from the unetched microstructure of this region, and the chemical compositions of points 1 and 2 in Table 6 show slight variation in the aluminium and copper contents. The composite like structure at the upper region of the Cu-stir zone (rectangle (ii)) resulted in two different contents of Al/Cu as illustrated in Fig. 8 (c) and Table 7. The higher heat input (1400 rpm) and the tool stirring action formed similar variation in Al/Cu at the bottom of Cu-stir zone as shown in Fig. 8 (d) of rectangle (iii). The dark shaded layers that surrounded the copper particles and accompanied the formation of Al/Cu IMCs are shown by the arrows.

3.3. *Interfacial elemental diffusion*

The key factor to critically analysing the joint quality in FSW of dissimilar aluminium to copper is by characterising the structure of the interfacial region [31]. The elemental diffusion and structure is able to confirm a reliable joint [20]. Fig. 9 (a) represents a magnified view of the interfacial region between the aluminium and the stir zone of test no. 4 at

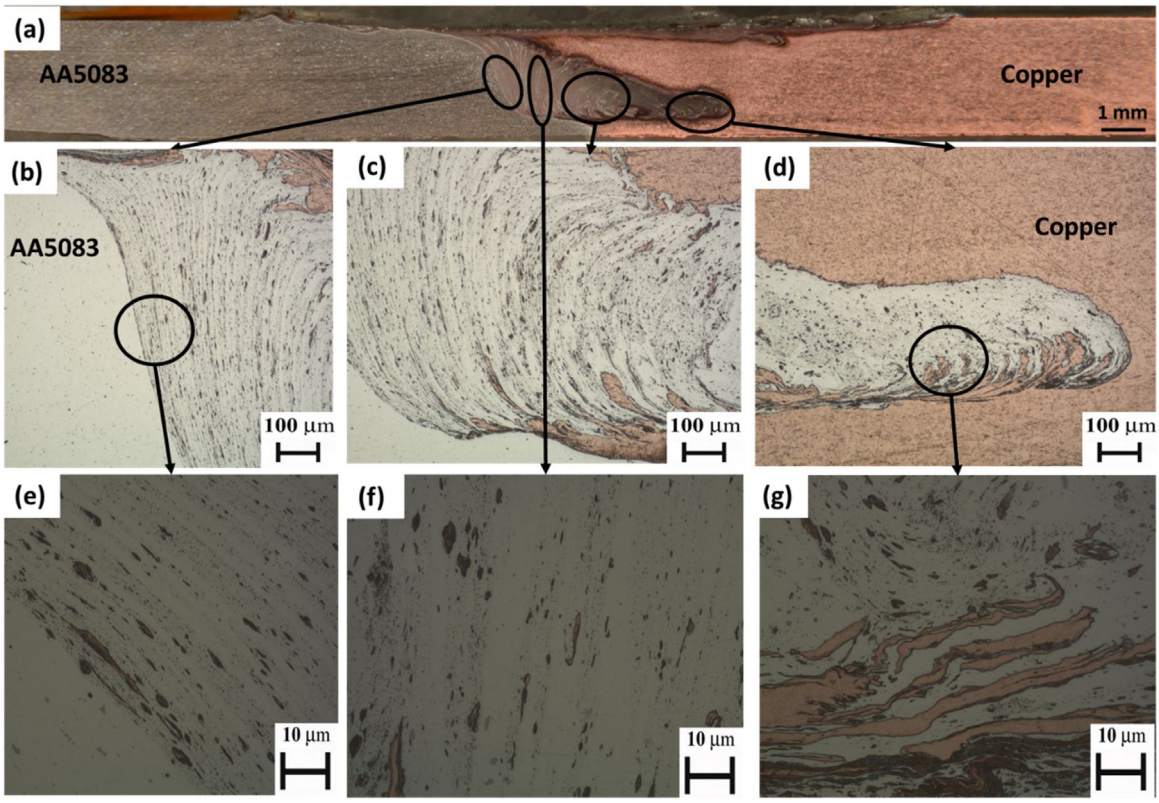

Fig. 5 – (a) Typical cross-section of joint welded at 1000 rpm and 100 mm/min. (b&e) interface zone towards AA5083 side. (c&f) stir zone. (d&g) interface zone towards the copper side.

1200 rpm tool rotational speed and 80 mm/min tool welding speed as etched by the aluminium etching solution. Continuous layers of refined aluminium grains are clearly observed. Copper particles with different sizes are diffused along with the refined layers of aluminium as evidence of good metallurgical bonding. The resultant stir zone, as shown in Fig. 9 (b), elucidates that the continuous interfacial layer subsequently leads to the lamella structure that significantly improves the joint mechanical strength.

The interfacial region formed a composite like structure as a result of increasing the heat input, as shown in Fig. 9 (c) of test no. 7 at 1400 rpm tool rotational speed and 80 mm/min tool welding speed. It has been reported previously [28] that the resultant joint strength is greatly improved by this structure. As it has been demonstrated in Fig. 9 (d), this composite like structure was also dominant inside the stir zone.

3.4. *Intermetallic phases*

XRD analysis was performed through the cross-sections to identify the phases present in the stir zone. Fig. 10 presents the XRD patterns of three typical defect- free joints of test no. 2, 4 and 7 of Table 4. The dominant IMCs on the stir zone of AA5083 and copper are Al2Cu and Al4Cu9, and these are confirmed from the three patterns, apart from the fact that AlCu was only detected under test no. 7. According to the above microstructure analysis of test no. 2 and 7, it can be established that the nature and quantity of IMCs are affected by the weld conditions. Peak intensity changes by varying the welding conditions, where 1000 rpm and 100 mm/min, 1200 rpm and 80 mm/min and 1400 rpm and 80 are the tool rotational speed and tool welding speed of test no. 2, 4 and 7 respectively. As observed, the peak intensity increases by increasing the tool rotational speed. It has been previously reported [22] that the variation of the intensity peaks is attributed to the complex mixing between Al-Cu overall, where relatively high intensity peaks indicate a higher IMC quantity [34].

According to the Al-Cu phase diagram, the formation temperature Al2Cu phase is relatively low [18]. Therefore, it is expected that Al2Cu will be present in the stir zone as the temperature during welding is known to reach 0.8–0.9 of the aluminium melting temperature [26], i.e. exceeding the formation temperature of Al_2Cu. However, the IMCs cannot be exclusively predicted on the basis of an Al-Cu phase diagram, where the chemical reactions occurring during the FSW under the thermal cycles are far from the equilibrium condition [18]. In the case of Al4Cu9, the thermomechanical effect of FSW explains its formation at the stir zone, where the melting temperature of this IMC i.e. 1030 °C [28] is higher than the peak temperature during FSW.

3.5. *Microhardness distribution*

Fig. 11 demonstrates the Vickers hardness distribution profiles of dissimilar joints measured across and at the middle of the weld cross-section. It is observed that the hardness value increases significantly at the stir zone relative to the base metals due to the presence of the IMCs which are hard and brittle

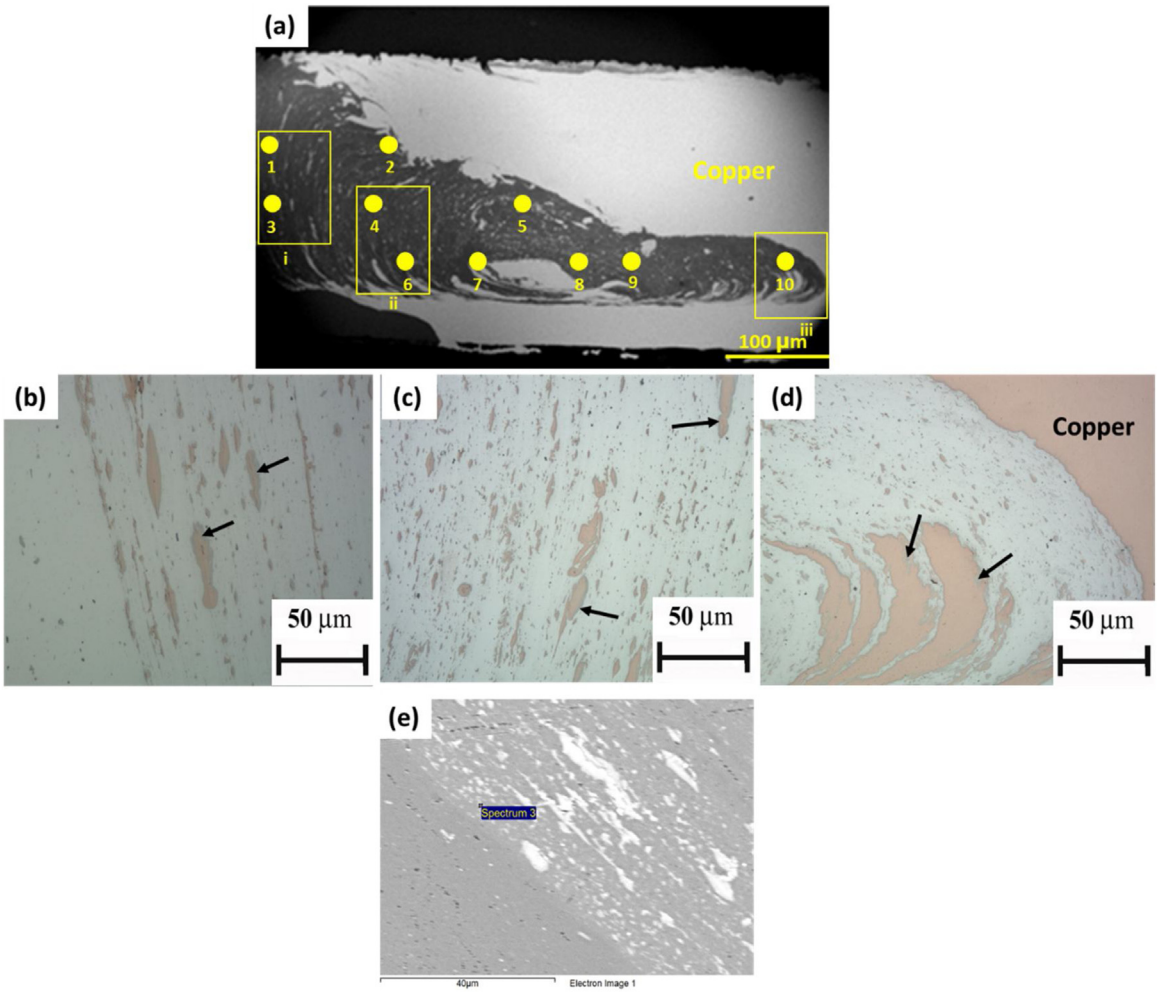

Fig. 6 – (a) SEM image and EDS points at the weld zone of Test no. 2. Magnified view of specific regions in Fig. 6(a): (b) region i, (c) region ii, (d) region iii, (e) region i.

in nature [34], accompanied with the formation of very fine recrystallised grains and copper-rich dispersed particles.

On the other hand, the combined effect of IMC formation and grain refinement due to the recrystallisation increases the hardness at the TMAZ. The HAZ in dissimilar FSW of aluminium to copper is mildly affected by the recrystallisation; this reduces the hardness in both HAZ sides [31]. The hardness variations are a direct result of the heterogeneous distribution of IMCs along with the softer materials (aluminium or copper) within the stir zone.

3.6. *Joint mechanical strength*

The performance of the dissimilar joints has been evaluated by assessing the tensile properties. Fig. 12 shows the yield strength, UTS and joint efficiency at the conditions that developed defect-free joints. Unlike other published work [28–30], placing the softer material (AA5083) on the advancing side resulted in higher tensile strength. The increase in tensile properties can be directly linked to the nature and quantity of IMCs in addition to the evolved microstructure, where proper material mixing is required to enhance the joint mechanical performance [4]. Moreover, significant improvements in the joint tensile properties were achieved compared to other studies that placed the softer material (aluminium) on the AS [32–35].

It is revealed from Fig. 12 that the effect of the tool rotational speed, in general, is higher than the effect of the welding speed, as this increases the heat input and subsequently improves the level of inter-mixing. Increasing the welding speed for the same level of tool rotational speed results in minor improvements in the joint UTS. The evolution of the composite-like structure that was produced at a higher level of tool rotational speed (1400 rpm) is the main reason for this improvement. The benefits of this structure on the joint strength have also been reported previously [26].

One of the most important criteria to identify the weld joint performance is by expressing the joint efficiency, i.e. the ratio of the weld tensile strength to the workpiece tensile strength, where a joint efficiency lower than 100% is generally reported during FSW of dissimilar aluminium/copper joints [31]. This efficiency is always relative to the lower UTS of aluminium base metal. In this work, high joint efficiency values

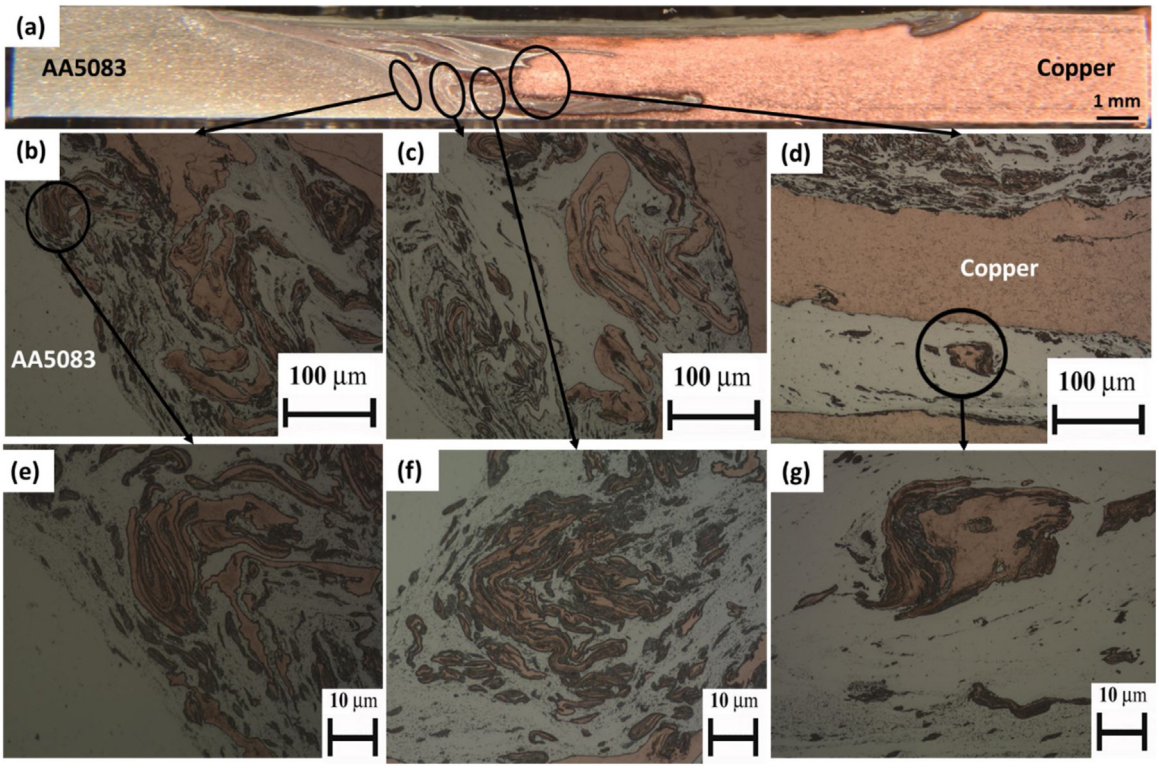

Fig. 7 – (a) Typical cross-section of joint welded at 1400 rpm and 80 mm/min. (b&e) interface zone towards AA5083 side. (c&f) stir zone. (d&g) interface zone towards copper side.

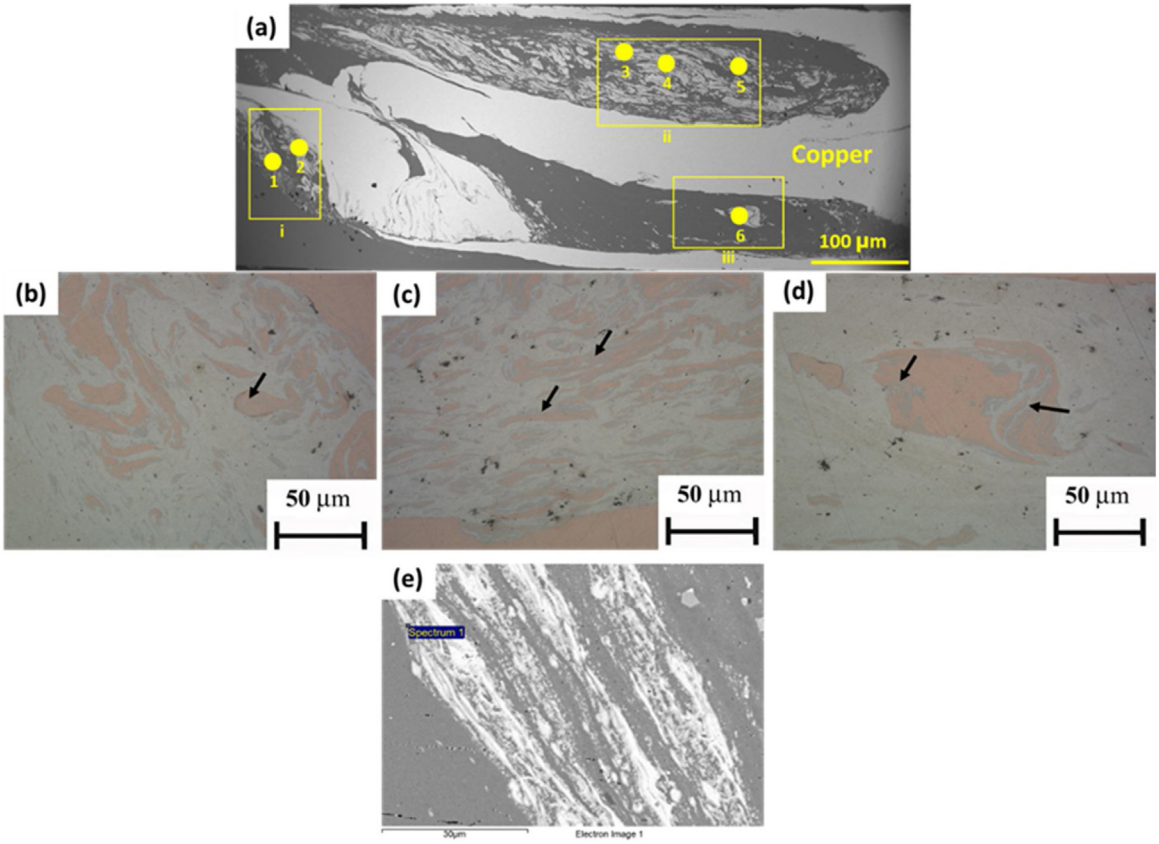

Fig. 8 – (a) SEM image and EDS points at the weld zone of condition no.7. (b) Enlarge view of regtanular i in Fig. 8 (a). (c) Enlarge view of regtanular ii in Fig. 8 (a). (d) Enlarge view of regtanular iii in Fig. 8 (a). (e) Enlarge SEM image of regtanular i in Fig. 8 (a).

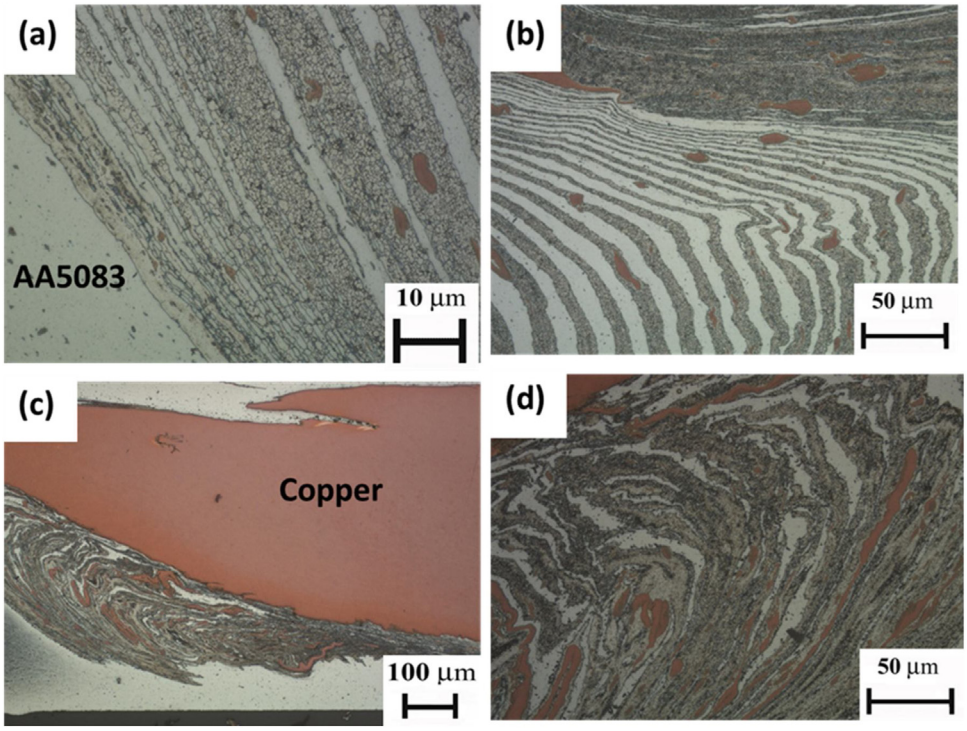

Fig. 9 – (a) Interfacial microstructure of the joint produced at test no. 4. (b) Lamella structure inside the stir zone at test no. 4. (c) Interfacial microstructure of the joint produced at test no. 7. (d) Composite like structure inside the stir zone at test no. 7.

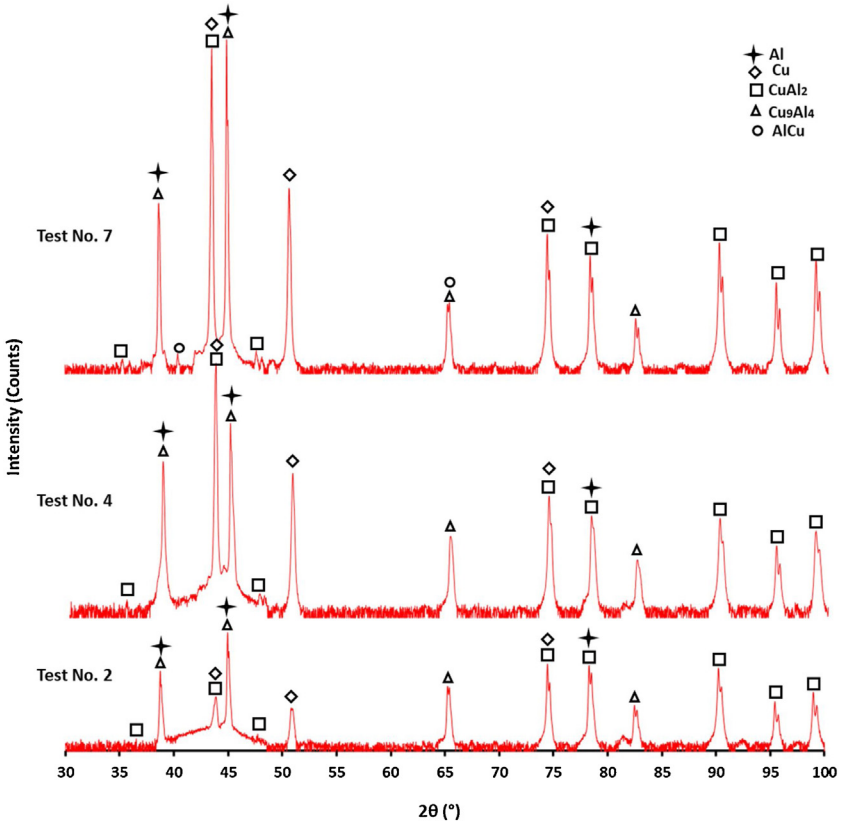

Fig. 10 – XRD patterns acquired under tests no. 2, 4 and 7.

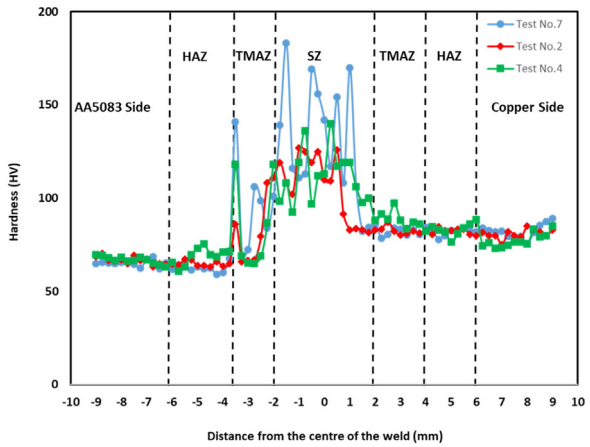

Fig. 11 – Hardness distribution under tests no. 2, 4 and 7.

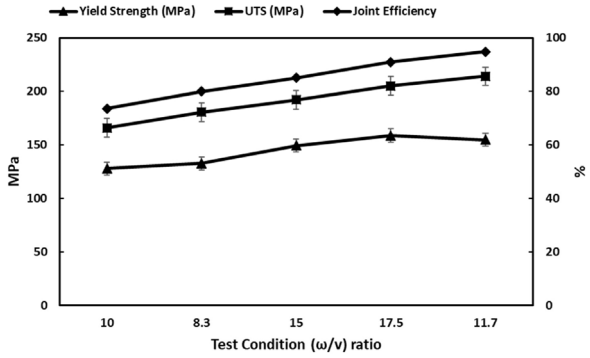

Fig. 12 – Yield strength, UTS and joint efficiency at different welding conditions.

were achieved at the conditions that yielded defect-free joints. Up to 94.8% joint efficiency was calculated at 1400 rpm and 120 mm/min, which is higher than the previously reported efficiency of 75.6% when considering the softer material on the advancing side [32].

The typical fracture surface for three different welding conditions is shown in Fig. 13. Failure occurred at the AS-TMAZ at the relatively low rotational speed of 1000 rpm and 100 mm/min welding speed (Fig.13 (a&d)). The failure location gradually shifted to the AS-HAZ by increasing the rotational speed as in Fig. 13 (b&e) and (c&f) of 1200 rpm-80 mm/min and 1400 rpm-80 mm/min, respectively. This change in failure location, shifting away from the weld zone and towards the AA5083 parent material is in full agreement with the gradual increase in joint efficiency, as displayed in Fig. 12.

4. Conclusions

FSW of AA5083 to commercially pure copper was experimentally investigated and the conditions that resulted in successful joints were identified. The following conclusions are drawn from the results of the present study:

- A successful weld joint between the two dissimilar materials has been achieved at different rotational and traverse speeds, where the harder material (copper) was placed at the retreating side without any tool offset.
- An inhomogeneous microstructure was observed inside and on the interfacial zone, when copper particles detached and intermixed with the aluminium matrix.
- A composite like structure was observed at a higher level of rotational speed and lamella or dispersed structures were found at the low level of rotational speed.
- The predominant intermetallic compounds at the aluminium-copper joint were Al2Cu and Al4Cu9.
- The volume fraction of the IMCs inside the stir zone increased by increasing the tool rotational speed as confirmed by the high XRD peak intensities and higher hardness values.

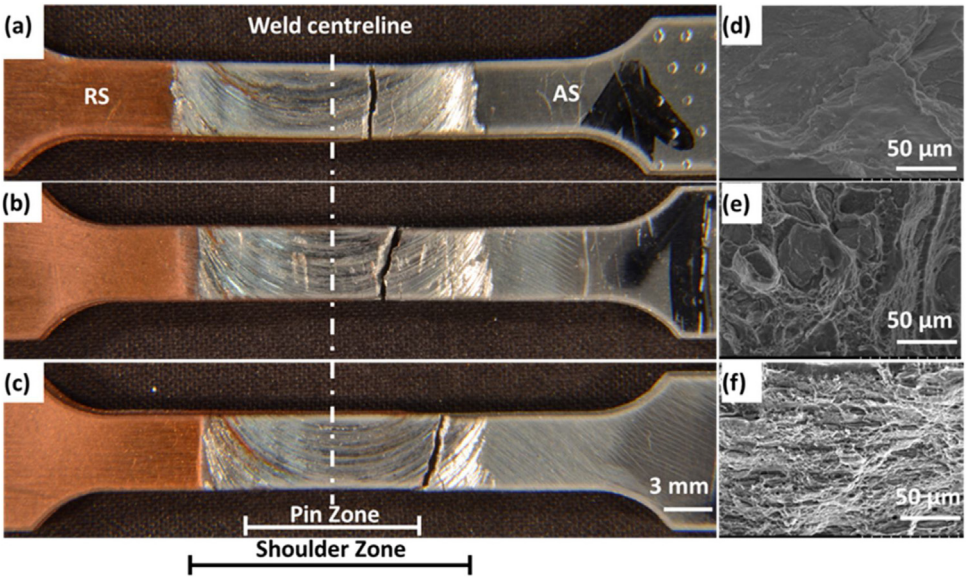

Fig. 13 – Fratography of the welds at tests no. 2 (a&d), 4 (b&e) and 7 (c&f).

- The UTS reached 203 MPa, representing a joint efficiency of 94.8% of the aluminium alloy as a result of the composite like structure and of an excellent metallurgical bond.

Conflicts of interest

The authors declare no conflicts of interest.

Acknowledgements

The authors acknowledge that part of this work was carried out at the Advanced Materials Research Laboratory, housed within the University of Strathclyde.

REFERENCES

[1] Bang HS, Bang HS, Jeon GH, Oh IH, Ro CS. Gas tungsten arc welding assisted hybrid friction stir welding of dissimilar materials Al6061-T6 aluminum alloy and STS 304 stainless steel. Mater Des 2012;37:48–55.
[2] Liu HJ, Shen JJ, Zhou L, Zhao YQ, Liu C, Kuang LY. Microstructural characterisation and mechanical properties of friction stir welded joints of aluminium alloy to copper. Sci. Technol. Weld. Join 2011;16(1):92–8.
[3] Xia C, Li Y, Puchkov UA, Gerasimov SA, Wang J. Microstructure and phase constitution near the interface of Cu/Al vacuum brazing using Al–Si filler metal. Vacuum 2008;82:799–804.
[4] Kumar N, Yuan W, Mishra RS. Introduction. Frict. Stir Weld. Dissimilar Alloy. Mater 2015:1–13.
[5] Wu CT, Hu W, Wang H-P, Lu H. A robust numerical procedure for the thermomechanical flow simulation of friction stir welding process using an adaptive element-free galerkin method. Math. Probl. Eng 2015;2015:16.
[6] Mofid M, Loryaei E. Investigating microstructural evolutionat the interface of friction stir weld and diffusion bond of Aland Mg alloys. J Mater Res Technol 2019.
[7] Eslami P, Taheri AK. An investigation on diffusion bonding of aluminum to copper using equal channel angular extrusion process. Mater Lett 2011;65:1862–4.
[8] Elnabi MMA, Elshalakany AB, Osman TA, El Mokadem A. Influence of friction stir welding parameters on metallurgical and mechanical properties of dissimilar AA5454 – AA7075 aluminum alloys. J Mater Res Technol 2019;8:1684–93.
[9] Nia Ahmad Tavassolimanesh Ali Alavi. Investigating the properties of bimetallic aluminum-clad copper tubesproduced by friction stir welding. J Alloys Compd 2018;751:299–306.
[10] Dalgaard E, Wanjara P, Trigo G, Jahazi M, Comeau G, Jonas JJ. Linear friction welding of Al–Cu: part 2-Interfacial characteristics. Can Metall Quart 2011;50(4):360–70.
[11] Sedighi M, Honarpisheh M. Experimental study of through-depth residual stress in explosive welded Al–Cu–Al multilayer. Mater Des 2012;37:577–81.
[12] Niu P, Li W, Yang X, Vairis A. Effects of microstructural asymmetries across friction stir welded AA2024 joints on mechanical properties. Sci. Technol. Weld. Join 2018;23(1):58–62.
[13] Mozhaiskaya TM, Chekanova NT. Structure and properties of welded aluminum–copper joints. Met Sci Heat Treat 1990;32(12):938–9.
[14] Mehta KP, Badheka VJ. Hybrid approaches of assisted heating and cooling for friction stir welding of copper to aluminum joints. J Mater Process Technol 2017;239:336–45.
[15] Khojastehnezhad VM, Pourasl HH. Microstructural characterization and mechanical properties of aluminum 6061-T6 plates welded with copper insert plate (Al/Cu/Al) using friction stir welding. Trans. Nonferrous Met. Soc. China 2018;28(3):415–26.
[16] Sahu PK, Pal S, Pal SK. Al/Cu dissimilar friction stir welding with Ni, Ti, and Zn foil as the interlayer for flow control, enhancing mechanical and metallurgical properties. Metall. Mater. Trans. A Phys. Metall. Mater. Sci 2017;48(7): 3300–17.
[17] Sheng LY, Yang F, Xi TF, Lai C, Ye HQ. Influence of heat treatment on interface of Cu/Al bimetal composite fabricated by cold rolling. Compos Part B Eng 2011;42:1468–73.
[18] Ouyang J, Yarrapareddy E, Kovacevic R. Microstructural evolution in the friction stir welded 6061 aluminum alloy (T6-temper condition) to copper. J Mater Process Technol 2006;172(1):110–22.
[19] Abdollah-Zadeh A, Saeid T, Sazgari B. Weldability and mechanical properties of dissimilar aluminum-copper lap joints made by friction stir welding. J Alloys Compd 2008;460:535.
[20] Xue P, Ni DR, Wang D, Xiao BL, Ma ZY. Effect of friction stir welding parameters on the microstructure and mechanical properties of the dissimilar Al–Cu joints. Mater. Sci. Eng. A 2011;528(13–14):4683–9.
[21] Galvão I, Leal RM, Loureiro A, Rodrigues DM. Material flow in heterogeneous friction stir welding of aluminium and copper thin sheets. Sci. Technol. Weld. Join 2010;15(8):654–60.
[22] Bakhtiari Argesi F, Shamsipur A, Mirsalehi SE. Dissimilar joining of pure copper to aluminum alloy via friction stir welding. Acta Metall. Sin. (English Lett 2018;5.
[23] Genevois C, Girard M, Huneau B, Sauvage X, Racineux G. Interfacial reaction during friction stir welding of Al and Cu [J]. Metall Mater Trans A 2011;42(8):2290.
[24] Liu HJ, Shen JJ, Zhou L, Zhao YQ, Liu C, Kuang LY. Microstructural characterisation and mechanical properties of friction stir welded joints of aluminium alloy to copper [J]. Sci Technol Weld Join 2011;16(1):92–8.
[25] Zhou L, Zhang RX, Li GH, Zhou WL, Huang YX, Song XG. Effect of pin profile on microstructure and mechanical properties of friction stir spot welded Al-Cu dissimilar metals. J Manuf Process 2018;36:1–9.
[26] Beygia R, Zarezadeh Mehrizia M, Verdera D, Loureiro A. Influence of tool geometry on material flow and mechanical properties of friction stir welded Al-Cu bimetals. J Mater Process Technol 2018:739–48.
[27] Bisadi H, Tavakoli A, Tour Sangsaraki M, Tour Sangsaraki K. The influences of rotational and welding speeds on microstructures and mechanical properties of friction stir welded Al5083 and commercially pure copper sheets lap joints. Mater Des 2013:80–8.
[28] Galvão I, Oliveira JC, Loureiro A, Rodrigues DM. Formation and distribution of brittle structures in friction stir welding of aluminium and copper: influence of shoulder geometry. Intermetallics 2012;22:122–8.
[29] Xue P, Xiao BL, Ni DR, Ma ZY. Enhanced mechanical properties of friction stir welded dissimilar Al-Cu joint by intermetallic compounds. Mater Sci Eng A 2010;21-21:5723–7.
[30] Regensburg Anna, Schürer René, Weigl Markus, Bergmann Jean Pierre. Influence of pin length and electrochemical platings on the mechanical strength and macroscopic defect formation in stationary shoulder friction stir welding of aluminium to copper. Metals 2018;2.
[31] Sharma N, Khan ZA, Siddiquee AN. Friction stir welding of aluminum to copper—An overview. Trans. Nonferrous Met. Soc. China (English Ed 2017;27(10):2113–36.
[32] Tan CW, Jiang ZG, Li LQ, Chen YB, Chen XY. Microstructural evolution and mechanical properties of dissimilar Al–Cu

joints produced by friction stir welding. Mater Des 2013;51:466–73.
[33] Shankar Sachindra, Vilaça Pedro, Dash Priyabrat, Chattopadhyaya Somnath, Hloch Sergej. Joint strength evaluation of friction stir welded Al-Cu dissimilar alloys. Measurement 2019;146:892–902.
[34] Liu P, Shi QY, Wang W, Wang X, Zhang ZL. Microstructure and XRD analysis of FSW joints for copper T2/aluminum 5A06 dissimilar materials. Mater Lett 2008;62:4106–8.
[35] Xu WF, Liu JH, Chen DL. Material flow and core/multi-shell structures in a friction stir welded aluminum alloy with embedded copper markers. J Alloys Compd 2011;509:8449–54.